Method for Estimating Harmonic Frequency Dependence of Diffusion Coefficient and Convective Velocity in Heat Pulse Propagation Experiment

Tatsuya Kobayashi[1], Kimitaka Itoh[1,2,3], Katsumi Ida[1,3], Sigeru Inagaki[3,4], and Sanae-I. Itoh[3,4]

[1] National Institute for Fusion Science, National Institutes of Natural Sciences, Gifu, Japan

[2] Institute of Science and Technology Research, Chubu University, Kasugai 487-8501, Japan

[3] Research Center for Plasma Turbulence, Kyushu University, Fukuoka, Japan

[4] Research Institute for Applied Mechanics, Kyushu University, Fukuoka, Japan

E-mail: kobayashi.tatsuya@LHD.nifs.ac.jp

Abstract. In this paper we propose a new set of formulae for estimating the harmonic frequency dependence of the diffusion coefficient and the convective velocity in the heat pulse propagation experiment in order to investigate the transport hysteresis. The assumptions that are used to derive the formulae can result in *dummy* frequency dependences of the transport coefficients. It is shown that these dummy frequency dependences of the transport coefficients can be distinguished from the true frequency dependence due to the transport hysteresis by using a *bidirectional* heat pulse propagation manner, in which both the outward propagating heat pulse and the inward propagating heat pulse are analyzed. The validity of the new formulae are examined in a simple numerical calculation.

1. Introduction

Quantitative prediction of plasma thermal transport is a crucial issue for the design work for the future commercial fusion reactor. Recently, clear evidence showing the emergence of a *hysteresis* in the flux-gradient relation was discovered [1-3], involving a rapid response of turbulence intensity and turbulent transport against the electron cyclotron resonance heating (ECH) [2]. A possible working hypothesis that can justify these observations has been proposed as an immediate interaction of the turbulence and the axial heating in phase-space [4]. This mechanism can also shed light on a long standing mystery, that is, the rapid increase of the electron thermal diffusivity in response to the ECH, found in the Wendelstein 7-AS stellarator [5]. The discovery of the hysteresis clarifies that the flux-gradient relation in the turbulent plasma is no longer a single-valued function, indicating the violation of the classical local transport model.

Perturbative experiments have been widely performed using heat pulses caused by either the modulation ECH (MECH) or the plasma instabilities. [1-3,6-13]. See also a review [14]. If the classical local transport model is valid, the higher harmonic components of the MECH electron temperature perturbation should have the faster amplitude radial decay than the fundamental component [14]. Meanwhile, under the existence of the hysteresis, the amplitude radial decay of the higher harmonic components is predicted to be slower and to approach that of the fundamental component [15, 16]. Recent experimental results support this prediction, showing almost constant amplitude radial decay rates in the fundamental perturbation component and

the higher harmonics [6, 7]. In these circumstances, the transport coefficients obtained from the perturbation experiment can have a frequency dependence if one attempts to fit the observation by the diffusion coefficient and the convective velocity. Therefore, the possible violation of the classical local transport model can be detected by investigating the harmonic frequency dependence of the transport coefficients. A set of formulae that gives the transport coefficients as a function of the harmonic frequency is desired.

There are several models to estimate the transport coefficients from the radial amplitude decay and the phase difference of the temperature perturbation [17-20]. However, in these methods the uniqueness of the transport coefficients is assumed in different frequencies, which is not generally proven, and more than two harmonic components are used to estimate the transport coefficients. In this paper, we propose a new set of formulae that estimate the transport coefficients using a single harmonic frequency of the temperature perturbation. With proper treatment of the higher order cylindrical coordinate correction, the true diffusion coefficient and the convective velocity can be successfully calculated at any harmonic frequency. The assumptions that are used to derive the formulae can result in *dummy* frequency dependences of the transport coefficients. To distinguish these dummy frequency dependences of the transport coefficients from the true frequency dependence, a *bidirectional* heat pulse propagation manner, in which both the outward propagating heat pulse and the inward propagating heat pulse are analyzed, is proposed. The validity of the new formulae are examined using a simple numerical calculation.

2. Model

We start from the one-dimensional thermal transport equation in the cylindrical coordinate for the (total) electron temperature T [17]

$$n_0 \frac{\partial T}{\partial t} + \frac{n_0 T}{\tau} = -\frac{1}{x}\frac{\partial (x q_x)}{\partial x} + S, \tag{1}$$

where, x, n_0, τ, q_x, and S are the radial coordinate, the unperturbed electron density, the damping term, the radial heat flux, and the source term, respectively. The radial heat flux is defined as

$$q_x = -n_0 \chi \nabla T + n_0 V T, \tag{2}$$

where χ and V are the diffusion coefficient and the convective velocity, respectively. Each of them is regarded to be a function of T and ∇T, and can be a function of radius. The perturbed component of the electron temperature $\tilde{T}$, in which the tilde denotes perturbed quantities, evolves

$$n_0 \frac{\partial \tilde{T}}{\partial t} + \frac{n_0 \tilde{T}}{\tau} = -\frac{1}{x}\frac{\partial (x \tilde{q}_x)}{\partial x} + \tilde{S}, \tag{3}$$

where, $T = T_0 + \tilde{T}$ and T_0 is the unperturbed electron temperature. We linearize the perturbation component of the radial heat flux by assuming a small amplitude of the temperature perturbation as

$$\tilde{q}_x = -n_0 \chi_{\mathrm{HP}} \nabla \tilde{T} + n_0 V_{\mathrm{HP}} \tilde{T}, \tag{4}$$

where χ_{HP} and V_{HP} are the heat pulse diffusion coefficient and the heat pulse convective velocity defined as

$$\chi_{\mathrm{HP}} = \chi + \frac{\partial \chi}{\partial \nabla T}\nabla T_0 - \frac{\partial V}{\partial \nabla T} T_0 \tag{5}$$

and

$$V_{\rm HP} = V - \frac{\partial \chi}{\partial T}\nabla T_0 + \frac{\partial V}{\partial T}T_0, \tag{6}$$

respectively [14]. At the radius where the modulation source term is not deposited, which we call the source-free region, the perturbed electron thermal transport equation in the cylindrical coordinate is obtained by substituting Eq. (4) into Eq. (3) as

$$n_0\frac{\partial \tilde{T}}{\partial t} = \frac{1}{x}\frac{\partial}{\partial x}\left(x n_0 \chi_{\rm HP}\frac{\partial \tilde{T}}{\partial x}\right) - \frac{1}{x}\frac{\partial}{\partial x}\left(x n_0 V_{\rm HP}\tilde{T}\right) - \frac{n_0\tilde{T}}{\tau}. \tag{7}$$

The WKB type solution

$$T = T_0 \exp(-i\omega t + i\int k dx) \tag{8}$$

is considered, where ω is the angular frequency and k is the complex wavenumber $k = k_{\rm r} + ik_{\rm i}$. The real part and the imaginary part of the radial wavenumber are defined as $k_{\rm i} = -A'/A$ and $k_{\rm r} = \phi'$, where A and ϕ denote the radial profiles of the perturbation amplitude and the phase, respectively. The dispersion relation can be obtained as

$$\begin{aligned} -i\omega = &-\chi_{\rm HP}k^2 - iV_{\rm HP}k + i\chi_{\rm HP}\frac{k}{x} - \frac{V_{\rm HP}}{x} + i\chi_{\rm HP}k' \\ &-\frac{1}{L_n}\left(i\chi_{\rm HP}k - V_{\rm HP}\right) + i\chi'_{\rm HP}k - V'_{\rm HP} - \frac{1}{\tau}, \end{aligned} \tag{9}$$

where $L_n = -n_0/n'_0$ is the scale length of the density gradient. Four terms from the end of the r.h.s. account for the spatial inhomogeneity in n_0, $\chi_{\rm HP}$, and $V_{\rm HP}$, and the finite damping term, respectively.

For simplicity, we first consider the case where these effects can be neglected. The dispersion relation Eq. (9) becomes

$$-i\omega = -\chi_{\rm HP}k^2 - iV_{\rm HP}k + i\chi_{\rm HP}\frac{k}{x} - \frac{V_{\rm HP}}{x} + i\chi_{\rm HP}k'. \tag{10}$$

If one derives the dispersion relation in the slab geometry, only the first two terms survive in the r.h.s., giving a characteristic wavenumber

$$k_0 = -i\frac{V_{\rm HP}}{2\chi_{\rm HP}} \pm \sqrt{i\frac{\omega}{\chi_{\rm HP}} - \left(\frac{V_{\rm HP}}{2\chi_{\rm HP}}\right)^2}, \tag{11}$$

where the positive sign and the negative sign in front of the square root account for the outward propagation and the inward propagation of the heat pulse, respectively. The value of k_0 is independent on the radius. Taking into account the finite density gradient, the zeroth order wavenumber is modified as

$$k_0 = -i\left(\frac{V_{\rm HP}}{2\chi_{\rm HP}} + \frac{1}{2L_n}\right) \pm \sqrt{i\frac{\omega}{\chi_{\rm HP}} - \left(\frac{V_{\rm HP}}{2\chi_{\rm HP}} - \frac{1}{2L_n}\right)^2}. \tag{12}$$

Under the condition $|(k_0 x)^{-1}| \ll 1$, Eq. (10) is subject to the perturbative expansion for k as

$$k = k_0\left[1 + i\frac{C_1}{k_0 x} + \frac{C_2}{k_0^2 x^2} + i\frac{C_3}{k_0^3 x^3} + \frac{C_4}{k_0^4 x^4} + i\frac{C_5}{k_0^5 x^5}\right], \tag{13}$$

with the order parameter $(k_0 x)^{-1}$. Note that the condition $|(k_0 x)^{-1}| \ll 1$ is satisfied widely in MECH experiments, e.g., Ref. [2]. The third term and the fourth term of Eq. (10) are the first order correction with respect to the slab approximation. The last term of Eq. (10) regarding k' is the second order correction since the zeroth order of the wavenumber k_0 is independent on the radius. We truncate the perturbative approach up to the fifth order. See the derivation of the formula and the explicit expressions of the coefficients in Appendix A.

Transport coefficients $\chi_{\rm HP}$ and $V_{\rm HP}$ can be obtained from the real part and the

imaginary part of Eq. (10) as a function of the frequency and the wavenumber as,

$$\chi_{\mathrm{HP}} = \chi_{\mathrm{c}} \left(1 - \epsilon + \epsilon^2\right) \tag{14}$$

and

$$V_{\mathrm{HP}} = V_{\mathrm{c}} \left(1 - \epsilon + \epsilon^2\right) + \chi_{\mathrm{c}} \frac{k_{\mathrm{i}}'}{k_{\mathrm{i}}\gamma} \left(1 - \epsilon\right), \tag{15}$$

respectively. The parameters χ_{c} and V_{c} show the diffusion coefficient and the convective velocity with the first order cylindrical correction given as

$$\chi_{\mathrm{c}} = \frac{1}{k_{\mathrm{r}}^2 + k_{\mathrm{i}}^2\gamma^2} \frac{k_{\mathrm{i}}\gamma}{k_{\mathrm{r}}} \omega, \tag{16}$$

and

$$V_{\mathrm{c}} = \frac{k_{\mathrm{r}}^2 - k_{\mathrm{i}}^2\gamma}{k_{\mathrm{r}}^2 + k_{\mathrm{i}}^2\gamma^2} \frac{1}{k_{\mathrm{r}}} \omega, \tag{17}$$

respectively. The factors γ and ϵ show the first order and the second order of the cylindrical geometry corrections, which are given as

$$\gamma = 1 - \frac{1}{k_{\mathrm{i}} x} \tag{18}$$

and

$$\epsilon = \frac{-\frac{k_{\mathrm{i}}\gamma}{k_{\mathrm{r}}} k_{\mathrm{r}}' + k_{\mathrm{i}}'}{k_{\mathrm{r}}^2 + k_{\mathrm{i}}^2\gamma^2}, \tag{19}$$

respectively. See Appendix B for the derivation of Eqs. (14) and (15). The radial derivative of the wavenumber may be difficult to obtain from the experimental data due to the noise issue. Instead, we evaluate k' terms by use of Eq. (13) as

$$k' = -k_0 \left[i \frac{C_1}{k_0 x^2} + 2 \frac{C_2}{k_0^2 x^3} + i3 \frac{C_3}{k_0^3 x^4} + 4 \frac{C_4}{k_0^4 x^5} \right], \tag{20}$$

where the coefficients C_i $(i = 1, 2, 3, 4)$ are obtained using χ_{c} and V_{c} at the first step. Then the newly obtained χ_{HP} and V_{HP} are again used to obtain more plausible C_i, in

order to obtain the more plausible $\chi_{\rm HP}$ and $V_{\rm HP}$ (iterative approach). If one does not take into account the higher order terms, the evaluated transport coefficients suffer large errors at the low frequency region or at the inner radial position.

3. Numerical Simulation

In order to demonstrate the validity of the proposed method, we perform a set of numerical studies that examine how the heat pulse propagates in the cylindrical coordinate.

We solve the transport equation Eq. (1) with the radial heat flux Eq. (2) using the "Crank-Nicolson method" [9, 21] in the cylindrical coordinate. Here, the transport coefficients are taken as constant against either T or ∇T, therefore $\chi = \chi_{\rm HP}$ and $V = V_{\rm HP}$. The parameters in the simulation are scaled to be realistic values of high temperature torus plasmas in the SI units. Boundary condition at the core region is defined as $\partial T/\partial x = 0$. The convection term in $x < 0.1$ m is forced to be zero. Outside the plasma radius $a = 0.6$ m, i.e., $x > a$, a buffer region with a strong outward convection term of $V > 30$ m/s is set, in which a heat sink at the scrape off layer (SOL) is simulated. The outermost point of the simulation is $a = 0.7$ m, in which the temperature is forced to be $T = 0$. The choice of the boundary condition does not affect the results of the perturbation experiment if the observation radius is not too close to the boundaries. The discussion for the boundary condition will be given in Sec. 4. The density profile is taken as constant in time and space. Two types of heating schemes are

simulated, i.e., the delta function type ECH and the Gaussian type Ohmic or Neutral Beam (NB) heating. By using the Fourier decomposition, the amplitude profile and the phase profile are obtained, by which the real part and the imaginary part of the wavenumber are fitted.

As an example, the results of the numerical simulation with the transport coefficients of $\chi_{\mathrm{HP}} = 4\ \mathrm{m}^2/\mathrm{s}$ and $V_{\mathrm{HP}} = -5\ \mathrm{m/s}$ (inward pinch) are shown, where the radial dependence of the transport coefficients and the finite value of τ are not taken into account. The radial profiles of the heating power and the given transport coefficients are shown in Figs. 1 (a) and (b). The input power of the NB is 1 MW. A modulation ECH (MECH), 50 % duty cycle block wave with the frequency of 20 Hz, is deposited at the very core region, $x = 0.05$ m. The 100 % modulation with the amplitude of 1 MW peak to peak is applied. Outward propagating heat pulse is analyzed at $x = 0.3$ m. A typical time evolution of the electron temperature profile is shown in Fig. 2. A time period $1\ \mathrm{s} \leq t \leq 3\ \mathrm{s}$ is analyzed where the temperature reaches the saturated profile as shown in Fig. 1 (c). The Fourier decomposition is performed to obtain the radial profiles of the electron temperature modulation power (square root of the amplitude) and the phase difference with respect to the MECH cycle. Shown in Fig. 3 is the result of the Fourier analysis for the fundamental frequency and the third, fifth, and seventh harmonic frequencies. A red shaded area at $x > 0.6$ m corresponds to the scrape off layer, in which a large outward convective velocity is applied. Except for the core region and the edge region, the power spectrum and the phase difference are almost on straight

lines, i.e., almost constant k_i and k_r are expected. On the contrary, the boundaries deform the heat pulse propagation. The linear fitting of the power profile and the phase profile provide the wavenumbers k_i and k_r at the radius of interest $x = 0.3$ m, from which the transport coefficients can be analyzed using Eqs. (14) and (15).

The formulae we obtained are then examined by the numerical simulation. Here, the plasma radius is doubled to reduce the outer boundary effect on the heat pulse propagation. Figures 4 (a), (b), and (c) show obtained k_i, k_r, and γ as a function of the frequency. The green curves show the expected wavenumbers given by Eq. (13). The order parameter $(k_0 x)^{-1}$ is smaller than unity at $f > 5$ Hz, and monotonically decreases as the frequency increases. Figures 4 (d) and (e) show the evaluated transport coefficients χ_HP and V_HP. The error bars are calculated using Eqs. (35) and (36) (see Appendix C) from the scatter of the wavenumbers δk_i and δk_r. For comparison, the transport coefficients are also evaluated with $\epsilon = 0$ and $\gamma = 1$ and with $\epsilon = 0$, i.e., neglecting the first order and the second order cylindrical coordinate corrections, respectively. With $\epsilon = 0$ and $\gamma = 1$, the obtained value of V_HP has a large negative offset. Even with the value of γ given by Eq. (18), the obtained transport coefficients have frequency dependences unless considering the correction of ϵ. By considering the cylindrical coordinate corrections, the evaluation errors are drastically reduced, and the given diffusion coefficient and convective velocity can be successfully obtained at any harmonic frequency. The small deviation comes from more higher order contribution that we truncated in Eqs. (14) and (15).

4. Harmonic Frequency Dependence of the Transport Coefficients due to Other Origin

Using Eqs. (14) and (15), one can discuss whether there is a harmonic frequency dependence in the transport coefficients that is due to the transport hysteresis. However, there are still some sources that can provide the estimation error of the transport coefficients depending on the frequency. There are the plasma boundaries, the radially dependent transport coefficients, and the finite damping term. In this section, we study the harmonic frequency dependence of the transport coefficients due to these sources. A *bidirectional* heat pulse propagation analysis is proposed to distinguish the frequency dependence of the transport coefficients due to the hysteresis from that due to the other sources.

4.1. Boundary effect

At the plasma center or the plasma edge, the propagation of the imposed heat pulse is expected to be disturbed. When the radius of interest for the analysis is not far enough from the boundaries, the obtained transport coefficients can also suffer the boundary effect. The effective distance to the boundaries may depend on the wavelength of the heat pulse, and thus inversely depend on the frequency [19]. Therefore, the estimation error is expected to decrease at the higher harmonic frequency. Appendix D numerically shows the relation between the effective distance to the boundary and the estimation error of the wavenumber. Here we propose an asymptotic approach by means of both

the outward and inward propagating pulses, which we call the *bidirectional* heat pulse propagation to estimate the true values of the transport coefficients. At lower frequency, the estimated transport coefficients with Eqs. (14) and (15) suffer a relatively large amount of error. The amount of the error is considered to be different in the cases of the outward propagating pulse and the inward propagating pulse. At higher frequency, the estimation error becomes smaller and the transport coefficients estimated from both the outward and inward propagating pulses are expected to converge to the true value. By observing the convergence property of the transport coefficients against the harmonic frequency, the true values may be estimated.

We numerically examine the bidirectional heat pulse propagation manner. The heat pulse propagation is simulated in the plasmas with the radius of $a = 0.6$ m. Shown in Fig. 5 is the radial profile of the NB heating power and the ECH heating power for the bidirectional heat pulse propagation analysis. Two ECHs are deposited at two different radii, $x = 0.2$ m and 0.4 m, where the radius of interest for the transport coefficient analysis is $x = 0.3$ m. One at $x = 0.2$ m (noted as MECH) is modulated in time with the frequency of 20 Hz, and the other (noted as SECH) at $x = 0.4$ m is stationary inputted. Both have the time averaged input power of 0.5 MW. By exchanging the MECH and SECH depositions, both the outward and inward propagating pulses can be analyzed at the position between them, keeping the total heat input constant. A similar scheme is used in Refs. [22, 11]. Figure 6 shows the results of the bidirectional heat pulse propagation analysis obtained by Eqs. (14) and (15), indicating that the

evaluated values of $\chi_{\rm HP}$ and $V_{\rm HP}$ converge to the given value as the frequency increases. Even without knowing the precise edge boundary condition, one can determine the true transport coefficients as the converged values of the bidirectional heat pulse propagation experiment. The fact that the true transport coefficients can be evaluated by means of the bidirectional heat pulse propagation is robust for the specific choice of the edge boundary condition in the numerical simulation.

4.2. Radially dependent transport coefficients and finite damping term

If one attempts to obtain $\chi_{\rm HP}$ and $V_{\rm HP}$ using the dispersion relation including the radially dependent transport coefficients and the finite damping term Eq. (9), additional terms appear in Eqs. (14) and (15) as

$$\chi_{\rm HP,a} = \chi_{\rm HP} + \frac{1}{k_{\rm r}^2 + k_{\rm i}^2\gamma^2}\left[k_{\rm i}(\gamma-1)\chi'_{\rm HP} - V'_{\rm HP} - \frac{1}{\tau}\right] \tag{21}$$

and

$$V_{\rm HP,a} = V_{\rm HP} + \frac{1}{k_{\rm r}^2 + k_{\rm i}^2\gamma^2}\left[(k_{\rm i}^2 + k_{\rm r}^2)\chi'_{\rm HP} + k_{\rm i}(\gamma+1)V'_{\rm HP} + k_{\rm i}(\gamma+1)\frac{1}{\tau}\right]. \tag{22}$$

Under the existence of finite $\chi'_{\rm HP}$, $V'_{\rm HP}$ or τ, the transport coefficients calculated by Eqs. (14) and (15) suffer estimation errors. The impact of these terms except for the second term in Eq. (22) decreases at the higher harmonic frequencies since the denominators having a quadratic order of $k_{\rm i}$ and $k_{\rm r}$ grow faster than the numerators. Although Eqs. (21) and (22) cannot be directly evaluated, the bidirectional heat pulse propagation would be useful to estimate the true values of $\chi_{\rm HP}$ and $V_{\rm HP}$. Only the second term in Eq. (22) can be an offset of the evaluated $V_{\rm HP}$. That offset value slowly

approaches to $\chi'_{\rm HP}$ since $\gamma \to 1$ at a higher frequency regime. Note that the coefficients of Eqs. (13) and (20) do not contain the effect of $\chi'_{\rm HP}$, $V'_{\rm HP}$ nor τ. Therefore, the prediction of the wavenumber becomes inaccurate when large values of $\chi'_{\rm HP}$, $V'_{\rm HP}$ or τ^{-1} exist. In the case that the density gradient is unknown, the estimated transport coefficients suffer the error as well. This error due to the density gradient behaves similar to that due to $\chi'_{\rm HP}$ and $V'_{\rm HP}$, and the substitutions $\chi'_{\rm HP} \to \chi'_{\rm HP} - \chi_{\rm HP}/L_n$ and $V'_{\rm HP} \to V'_{\rm HP} - V_{\rm HP}/L_n$ give the expression involving the density gradient contribution.

The convergence property is examined by means of the numerical simulation. In order to focus on the errors due to finite $\chi'_{\rm HP}$, $V'_{\rm HP}$ or τ^{-1}, the boundary effect discussed above is desired to be suppressed. For this purpose, the plasma radius is again doubled as the case in Fig. 4. In the presence of a finite damping term of $\tau = 10$ ms, the transport coefficients are fitted using Eqs. (14) and (15). Two ECH sources, the MECH and the SECH, are deposited at $x = 0.45$ m ($x = 0.75$ m) and $x = 0.75$ m ($x = 0.45$ m) for the analysis of the outward (inward) propagating pulse at $x = 0.6$ m. Figure 7 shows the result of the transport coefficients estimation using the bidirectional heat pulse. Because of the finite τ, the obtained values show frequency dependences. However, at the high frequency regime, the obtained values converge to the given values. By observing the asymptotic behavior against the frequency, the true values of $\chi_{\rm HP}$ and $V_{\rm HP}$ can be estimated even with a finite value of τ.

The case involving the radially dependent $\chi_{\rm HP}$ and $V_{\rm HP}$ is also examined. The heating profile is the same as previous. The given radial profiles of $\chi_{\rm HP}$ and $V_{\rm HP}$ for

the simulation are shown in Fig. 8. At the radius of interest $x = 0.6$ m, $\chi'_{\rm HP} = 10$ m/s and $V'_{\rm HP} = 5$ s^{-1} are given. These values are in the same order with the experimentally determined values [13, 14]. (The experimentally determined values cover a relatively wide range.) Figure 9 shows evaluated transport coefficients. The evaluated value of $\chi_{\rm HP}$ from the outward pulse and inward pulse changes similarly, and the convergence feature of both results with respect to the frequency is somewhat ambiguous. The value of $V_{\rm HP}$ converges to a value including an offset due to $\chi'_{\rm HP}$ as predicted by the third term in Eq. (22).

5. Discussion and Summary

In theory, it is predicted that the higher the harmonic frequency reaches, the larger difference of the transport coefficients obtained from the outward propagating pulse and the inward propagating pulse become in the presence of the hysteresis [16]. When the hysteresis exists in the flux-gradient relation, higher harmonic components of the temperature perturbation tend to propagate with a weaker decay with respect to the local prediction. Deviation of the experimentally fitted wavenumber from the locally predicted values becomes larger at higher harmonic frequency, which makes the difference of the transport coefficients obtained from the outward propagating pulse and the inward propagating pulse larger. That feature is opposite to the frequency dependence due to the plasma boundaries, the radially dependent transport coefficients, or the finite damping term. By observing the asymptotic convergence property, it is

possible to judge whether the frequency dependence of the transport coefficients is due to the transport hysteresis or due to other reasons.

In this paper, we proposed a new set of formulae for estimating the harmonic frequency dependence of the diffusion coefficient and the convective velocity in the heat pulse propagation experiment in order to investigate the transport hysteresis. The assumptions that were used to derive the formulae can result in *dummy* frequency dependences of the transport coefficients. It was shown that these dummy frequency dependences of the transport coefficients can be distinguished from the true frequency dependence due to the transport hysteresis by using a *bidirectional* heat pulse propagation manner, in which both the outward propagating heat pulse and the inward propagating heat pulse are analyzed. The validity of the new formulae were examined by a simple numerical calculation.

Acknowledgments

The authors thank Drs. H. K. Park, G. S. Yun, T. E. Evans, C. Hidalgo and B. Ph. Van Milligen for useful discussions. Comments by Drs. M. Sasaki, Y. Kosuga, and K. Nagaoka are also acknowledged. The authors appreciate Drs. S. Sakakibara and A. Fujisawa for their strong support. This work is partly supported by the Grant-in-Aid for Scientific Research of JSPS (16H02442, 15H02336,15H02155).

Appendix A: Coefficients of the Heat Pulse Wavenumber Obtained by the Perturbative Expansion

The coefficients of the heat pulse wavenumber shown in Eq. (13) can be obtained by the perturbative expansion. Substituting Eq. (13) into Eq. (10) gives

$$\begin{aligned}
-i\omega = & -\chi_{\mathrm{HP}}k_0^2 - iV_{\mathrm{HP}}k_0 \\
& + \frac{1}{x}\left[ik_0\chi_{\mathrm{HP}}(-2C_1+1) + V_{\mathrm{HP}}(C_1-1)\right] \\
& + \frac{1}{x^2}\frac{1}{k_0}\left[k_0\chi_{\mathrm{HP}}(-2C_2+C_1^2) - iV_{\mathrm{HP}}C_2\right] \\
& + \frac{1}{x^3}\frac{1}{k_0^2}\left[ik_0\chi_{\mathrm{HP}}(-2C_3-2C_1C_2-C_2) + V_{\mathrm{HP}}C_3\right] \\
& + \frac{1}{x^4}\frac{1}{k_0^3}\left[k_0\chi_{\mathrm{HP}}(-2C_4-C_2^2+2C_1C_3+2C_3) - iV_{\mathrm{HP}}C_4\right] \\
& + \frac{1}{x^5}\frac{1}{k_0^4}\left[ik_0\chi_{\mathrm{HP}}(-2C_5-2C_1C_4-2C_2C_3-3C_4) + V_{\mathrm{HP}}C_5\right]. \qquad (23)
\end{aligned}$$

The coefficients are calculated in each order as

$$C_1 = \frac{V_{\mathrm{n}}}{V_{\mathrm{d}}}, \qquad (24)$$

$$C_2 = k_0\chi_{\mathrm{HP}}\frac{V_{\mathrm{n}}^2}{V_{\mathrm{d}}^3}, \qquad (25)$$

$$C_3 = -k_0^2\chi_{\mathrm{HP}}^2\frac{V_{\mathrm{n}}^2}{V_{\mathrm{d}}^5}(4k_0\chi_{\mathrm{HP}} + i3V_{\mathrm{HP}}), \qquad (26)$$

$$C_4 = -k_0^3\chi_{\mathrm{HP}}^3\frac{V_{\mathrm{n}}^2}{V_{\mathrm{d}}^7}(25k_0^2\chi_{\mathrm{HP}}^2 - 13V_{\mathrm{HP}}^2 + i36k_0\chi_{\mathrm{HP}}V_{\mathrm{HP}}), \qquad (27)$$

and

$$C_5 = -k_0^4\chi_{\mathrm{HP}}^4\frac{V_{\mathrm{n}}^2}{V_{\mathrm{d}}^9}\left[208k_0^3\chi_{\mathrm{HP}}^3 - 304k_0\chi_{\mathrm{HP}}V_{\mathrm{HP}}^2 + i(435k_0^2\chi_{\mathrm{HP}}^2V_{\mathrm{HP}} - 71V_{\mathrm{HP}}^3)\right], \qquad (28)$$

where

$$V_{\mathrm{d}} = 2k_0\chi_{\mathrm{HP}} + iV_{\mathrm{HP}} \qquad (29)$$

and

$$V_{\rm n} = k_0 \chi_{\rm HP} + i V_{\rm HP}. \tag{30}$$

Appendix B: Derivation of the Diffusion Coefficient and the Convective Velocity

First, we derive the diffusion coefficient and the convective velocity with the first order cylindrical correction, i.e., $\chi_{\rm c}$ and $V_{\rm c}$, respectively. The dispersion relation Eq. (10) is analyzed neglecting the second order correction term, i.e., the fifth term in the r.h.s. The real part and the imaginary part of the dispersion relation become

$$-\chi_{\rm c}\left(k_{\rm r}^2 - k_{\rm i}^2 + \frac{k_{\rm i}}{x}\right) + V_{\rm c}\left(k_{\rm i} - \frac{1}{x}\right) = 0 \tag{31}$$

and

$$-\chi_{\rm c}\left(2k_{\rm r}k_{\rm i} - \frac{k_{\rm r}}{x}\right) - V_{\rm c}k_{\rm r} + \omega = 0, \tag{32}$$

respectively. These two equations can be solved for $\chi_{\rm c}$ and $V_{\rm c}$ as Eqs. (16) and (17) with the parameter γ.

Leaving the second order correction term, the real part and the imaginary part of the dispersion relation become

$$-\chi_{\rm HP}\left(k_{\rm r}^2 - k_{\rm i}^2 + \frac{k_{\rm i}}{x}\right) + V_{\rm HP}\left(k_{\rm i} - \frac{1}{x}\right) - \chi_{\rm HP}k_{\rm i}' = 0 \tag{33}$$

and

$$-\chi_{\rm HP}\left(2k_{\rm r}k_{\rm i} - \frac{k_{\rm r}}{x}\right) - V_{\rm HP}k_{\rm r} + \chi_{\rm HP}k_{\rm r}' + \omega = 0, \tag{34}$$

respectively. Finally, $\chi_{\rm HP}$ and $V_{\rm HP}$ can be obtained by solving Eqs. (33) and (34) as Eqs. (14) and (15) with the parameter ϵ.

Appendix C: Error Propagation into the Transport Coefficients

Estimation errors of $k_{\rm i}$ and $k_{\rm r}$, denoted as $\delta k_{\rm i}$ and $\delta k_{\rm r}$, respectively, can be given by the linear fitting of radial profiles of the modulation power and phase. Assuming that $\delta k_{\rm i}$ and $\delta k_{\rm r}$ are independent, the estimation error of $\chi_{\rm HP}$ and of $V_{\rm HP}$ are given as

$$\delta\chi_{\rm HP} = \sqrt{\left(\frac{\partial\chi_{\rm HP}}{\partial k_{\rm i}}\delta k_{\rm i}\right)^2 + \left(\frac{\partial\chi_{\rm HP}}{\partial k_{\rm r}}\delta k_{\rm r}\right)^2} \tag{35}$$

and

$$\delta V_{\rm HP} = \sqrt{\left(\frac{\partial V_{\rm HP}}{\partial k_{\rm i}}\delta k_{\rm i}\right)^2 + \left(\frac{\partial V_{\rm HP}}{\partial k_{\rm r}}\delta k_{\rm r}\right)^2}, \tag{36}$$

respectively. Partial derivatives can be obtained from Eqs. (14) and (15) as

$$\frac{\partial\chi_{\rm HP}}{\partial k_{\rm i}} = \frac{k_{\rm r}^2 - k_{\rm i}^2\gamma^2}{k_{\rm r}(k_{\rm r}^2 + k_{\rm i}^2\gamma^2)^2}\omega, \tag{37}$$

$$\frac{\partial\chi_{\rm HP}}{\partial k_{\rm r}} = \frac{-3k_{\rm r}^2 k_{\rm i}\gamma - k_{\rm i}^3\gamma^3}{k_{\rm r}^2(k_{\rm r}^2 + k_{\rm i}^2\gamma^2)^2}\omega, \tag{38}$$

$$\frac{\partial V_{\rm HP}}{\partial k_{\rm i}} = \frac{-k_{\rm i}k_{\rm r}^2(1+3\gamma) + k_{\rm i}^3\gamma^2(1-\gamma)}{k_{\rm r}(k_{\rm r}^2 + k_{\rm i}^2\gamma^2)^2}\omega, \tag{39}$$

and

$$\frac{\partial V_{\rm HP}}{\partial k_{\rm r}} = \frac{-k_{\rm r}^4 + k_{\rm i}^4\gamma^3 + k_{\rm r}^2k_{\rm i}^2\gamma(3+\gamma)}{k_{\rm r}^2(k_{\rm r}^2 + k_{\rm i}^2\gamma^2)^2}\omega. \tag{40}$$

Appendix D: Effect of the Harmonic Frequency on the Estimation Error of the Wavenumber due to the Plasma Boundary

Here, we scan the effective distance to the boundaries by scanning the zeroth order wavenumber k_0 via given $\chi_{\rm HP}$ value. Figure 10 plots $\chi_{\rm HP}$ and x dependence of the evaluation error of the real part of the wavenumber defined as $\Delta k_{\rm r} = (k_{\rm r}^{\rm simulation} - k_{\rm r}^{\rm expected})/k_{\rm r}^{\rm expected}$, where $k_{\rm r}^{\rm simulation}$ and $k_{\rm r}^{\rm expected}$ denote the obtained value from the simulation and the expected value from Eq. (13), respectively. The edge boundary effect on the outer propagating pulse is discussed. Note that the inner boundary effect on the inward propagating pulse was also examined, and qualitatively similar results were obtained. To examine the frequency dependence as well, the plots are given for the fundamental frequency and the seventh harmonic frequency. Note that with the small value of $\chi_{\rm HP}$, the radial amplitude decay is too fast and the amplitude reaches down to the noise level at the edge side, in which the evaluated wavenumber scattered. For the sake of clarity, the region where the coherence is less than 0.9 are shaded out. The dashed curves on the contour indicates $x = k_0^{-1}$ and $a - k_0^{-1}$. The error becomes large when the radius approaches to the edge and the edge boundary effect becomes significant. The error is also large when either the frequency or $\chi_{\rm HP}$ is small. The same tendency is also seen in the imaginary part of the wavenumber. In addition to the edge side, the error is also large at the inner side, because the order parameter approaches to unity.

References

[1] K W Gentle, M E Austin, J C DeBoo, T C Luce, and C C Petty 2006 *Phys. Plasmas* **13** 012311

[2] S Inagaki, T Tokuzawa, N Tamura, S-I Itoh, T Kobayashi, K Ida, T Shimozuma, S Kubo, K Tanaka, T Ido, A Shimizu, H Tsuchiya, N Kasuya, Y Nagayama, K Kawahata, S Sudo, H Yamada, A Fujisawa, K Itoh and the LHD Experiment Group 2013 *Nucl. Fusion* **53** 113006

[3] K Ida, Z Shi, HJ Sun, S Inagaki, K Kamiya, JE Rice, N Tamura, PH Diamond, G Dif-Pradalier, XL Zou, K Itoh, S Sugita, OD Gürcan, T Estrada, C Hidalgo, TS Hahm, A Field, XT Ding, Y Sakamoto, S Oldenbürger, M Yoshinuma, T Kobayashi, M Jiang, SH Hahn, YM Jeon, SH Hong, Y Kosuga, J Dong and S-I Itoh 2015 *Nucl. Fusion* **55** 013022

[4] S-I Itoh and K Itoh 2012 *Sci. Rep.* **2** 860

[5] U Stroth, L Giannone, HJ Hartfuss, the ECH Group, and the W7-AS Team 1996 *Plasma Phys. Control. Fusion* **38** 611

[6] S Inagaki, S-I Itoh, K Itoh, N Kasuya, T Kobayashi, A Fujisawa, T Tokuzawa, K Ida, S Kubo, T Shimozuma, N Tamura, H Tsuchiya, Y Nagashima, K Kawahata, H Yamada, A Komori and LHD Experiment Group 2013 *Plasma Fusion Res.* **8** 1202173

[7] S Inagaki, S-I Itoh, K Itoh, K Ida, D López-Bruna, M A Ochand, T Estrada, B Ph van Milligen, C Hidalgo, and N Kasuya 2014 *Plasma Fusion Res.* **9** 1202052

[8] P Mantica, F De Luca, G Gorini, A Jacchia, GMJ Hogeweij, NJ Lopes Cardozo, GJ Kramer, and ACC Sips 1992 *Nucl. Fusion* **32** 2203

[9] L Giannone, V Erckmann, U Gasparino, HJ Hartfuss, G Kuhner, H Maassberg, U Stroth, and M Tutter 1992 *Nucl. Fusion* **32** 1985

[10] S D Song, X L Zou, G Giruzzi, W W Xiao, X T Ding, B J Ding, J L Ségui, D Elbèze, F Clairet, C Fenzi, T Aniel, JF Artaud, V Basiuk, F Bouquey, R Magne, E Corbel and the Tore Supra Team 2012 *Nucl. Fusion* **52** 033006

[11] J C DeBoo, C C Petty, A E White, K H Burrell, E J Doyle, J C Hillesheim, C Holland, G R

McKee, T L Rhodes, L Schmitz, SP Smith, G Wang and L Zeng 2012 *Phys. Plasmas* **19** 082518

[12] P Mantica, G Gorini, G M D Hogeweij, N J Lopes Cardozo, and A M R Schilham 2000 *Phys. Rev. Lett.* **85** 4534

[13] P Mantica, F Ryter, C Capuano, H U Fahrbach, F Leuterer, W Suttrop, Jan Weiland, and ASDEX-Upgrade Team 2006 *Plasma Phys. Control. Fusion* **48** 385

[14] N J Lopes Cardozo 1995 *Plasma Phys. Control. Fusion* **37** 799

[15] K Itoh, S-I Itoh, S Inagaki, N Kasuya, and A Fujisawa 2015 *J. Phys. Soc. Jpn.* **85** 014501

[16] K Itoh 2016 Proc. 26th IAEA Fusion Energy Conf. (Kyoto, Japan) *(Vienna: IAEA)* pages OV/P–8

[17] A Jacchia, P Mantica, F De Luca, and G Gorini 1991 *Phys. Fluids B* **3** 3033–3040

[18] M van Berkel, H J Zwart, N Tamura, G M D Hogeweij, S Inagaki, M R De Baar, and K Ida 2014 *Phys. Plasmas* **21** 112507

[19] M van Berkel, G M D Hogeweij, N Tamura, H J Zwart, S Inagaki, M R De Baar, and K Ida 2014 *Phys. Plasmas* **21** 112508

[20] M van Berkel, N Tamura, G M D Hogeweij, HJ Zwart, S Inagaki, M R de Baar, and K Ida 2014 *Phys. Plasmas* **21** 112509

[21] K S Riedel, A Eberhagen, O Gruber, K Lackner, G Becker, O Gehre, V Mertens, J Neuhauser, F Wagner, ASDEX Team, 1988 *Nucl. Fusion* **28** 1509

[22] F Ryter, G Tardini, F De Luca, H-U Fahrbach, F Imbeaux, A Jacchia, KK Kirov, F Leuterer, P Mantica, AG Peeters, G Pereverzev, W Suttrop and ASDEX Upgrade Team 2003 *Nucl. Fusion* **43** 1396

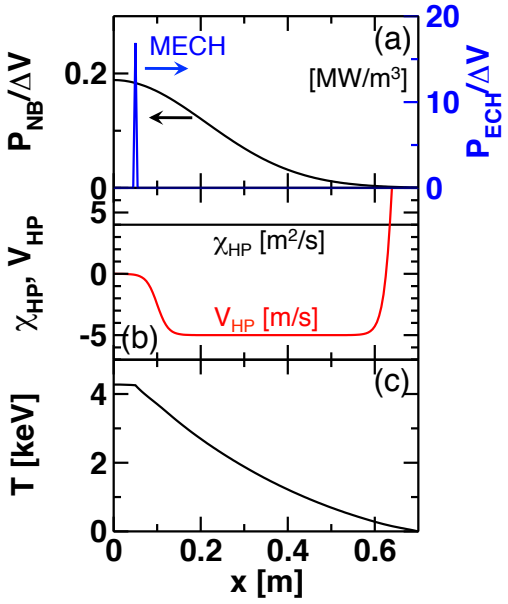

Figure 1. (Color online) Radial profiles of (a) the NB heating power and the ECH heating power, (b) the given $\chi_{\rm HP}$ and $V_{\rm HP}$, and (c) the mean electron temperature.

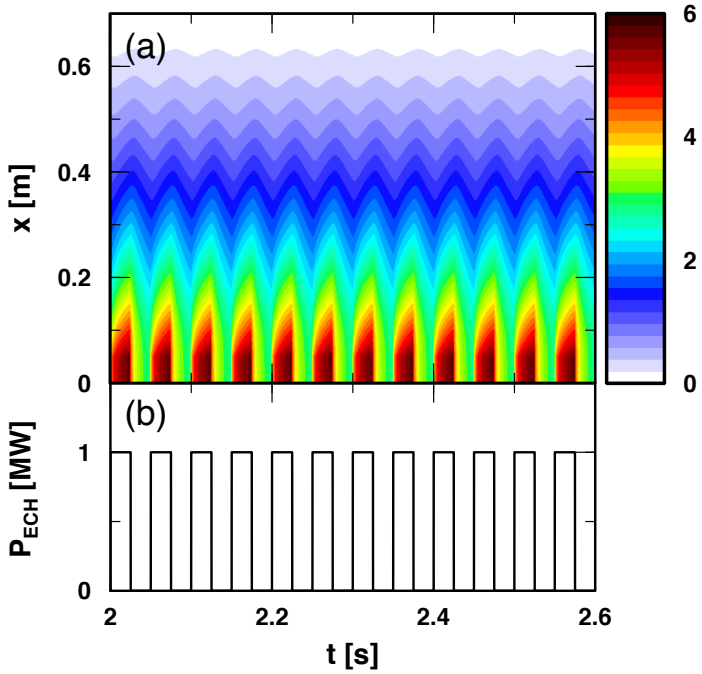

Figure 2. (Color online) (a) Spatiotemporal evolution of the electron temperature and (b) time evolution of the input MECH power.

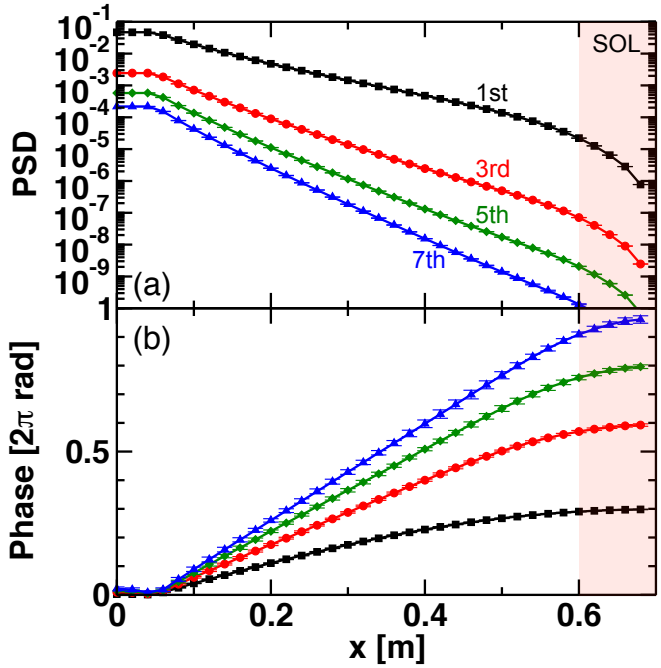

Figure 3. (Color online) Radial profiles of (a) the modulation power and (b) the modulation phase for the first, third, fifth, and seventh harmonics. Radius $x > 0.6$ m corresponds to the SOL, in which a strong outward convective velocity is set.

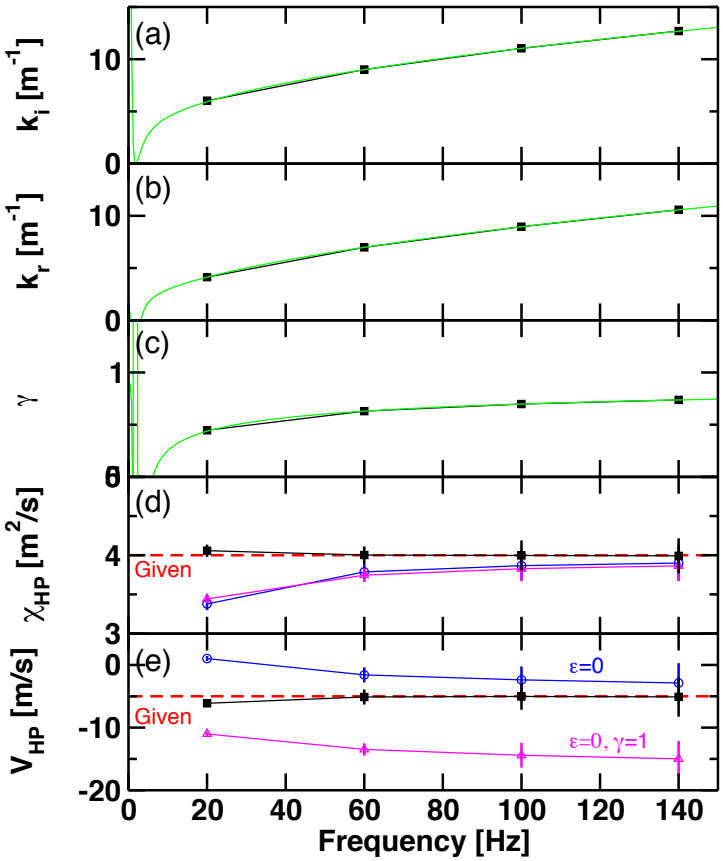

Figure 4. (Color online) Evaluation of the transport coefficients for the doubled radius simulation: frequency dependences of (a) the imaginary part of the wavenumber, (b) the real part of the wavenumber, (c) the cylindrical factor γ, (d) the evaluated $\chi_{\rm HP}$, and (e) the evaluated $V_{\rm HP}$.

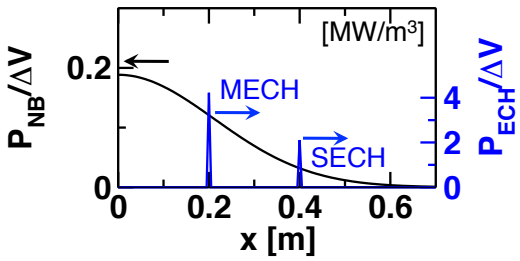

Figure 5. (Color online) Radial profiles of the NB heating power and the ECH heating power for the bidirectional heat pulse propagation analysis.

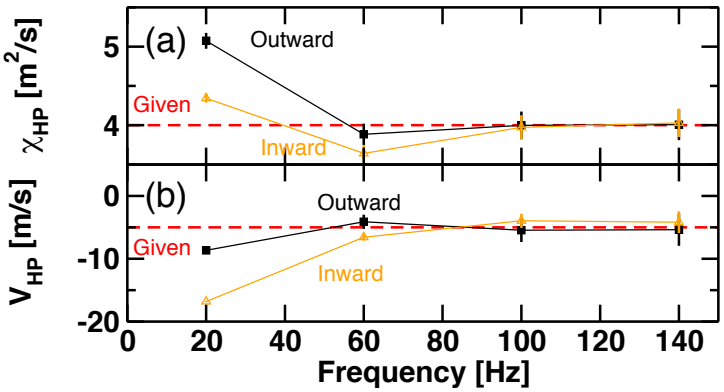

Figure 6. (Color online) Evaluation of the transport coefficients by the bidirectional manner in the presence of the edge boundary effect: frequency dependences of (a) the evaluated $\chi_{\rm HP}$ and (b) the evaluated $V_{\rm HP}$.

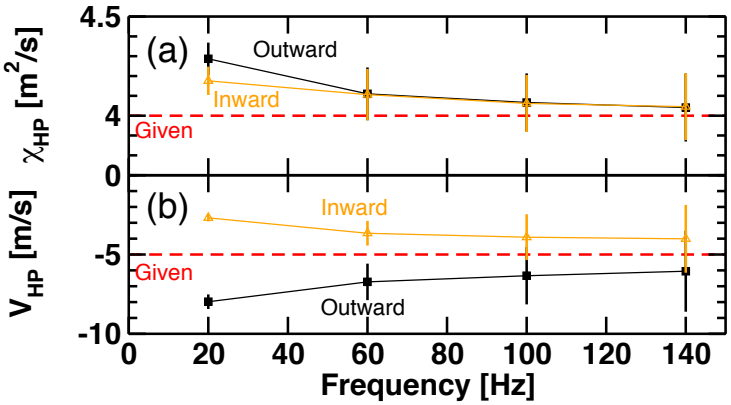

Figure 7. (Color online) Evaluation of the transport coefficients by the bidirectional manner in the presence of a finite damping term: frequency dependences of (a) the evaluated $\chi_{\rm HP}$ and (b) the evaluated $V_{\rm HP}$.

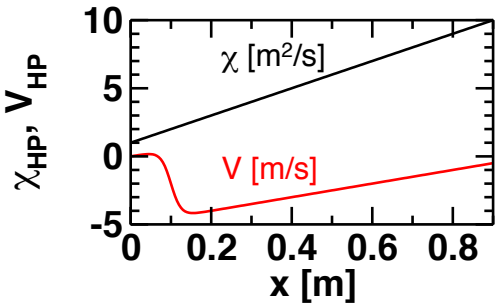

Figure 8. (Color online) Radial profiles of the given $\chi_{\rm HP}$ and $V_{\rm HP}$ in the case in which the transport coefficients depend on radius.

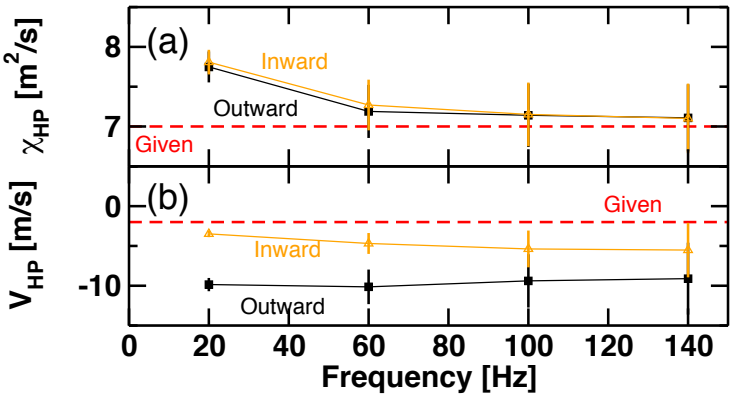

Figure 9. (Color online) Evaluation of the transport coefficients by the bidirectional manner in the presence of the radially dependent transport coefficients: frequency dependences of (a) the evaluated χ_{HP} and (b) the evaluated V_{HP}.

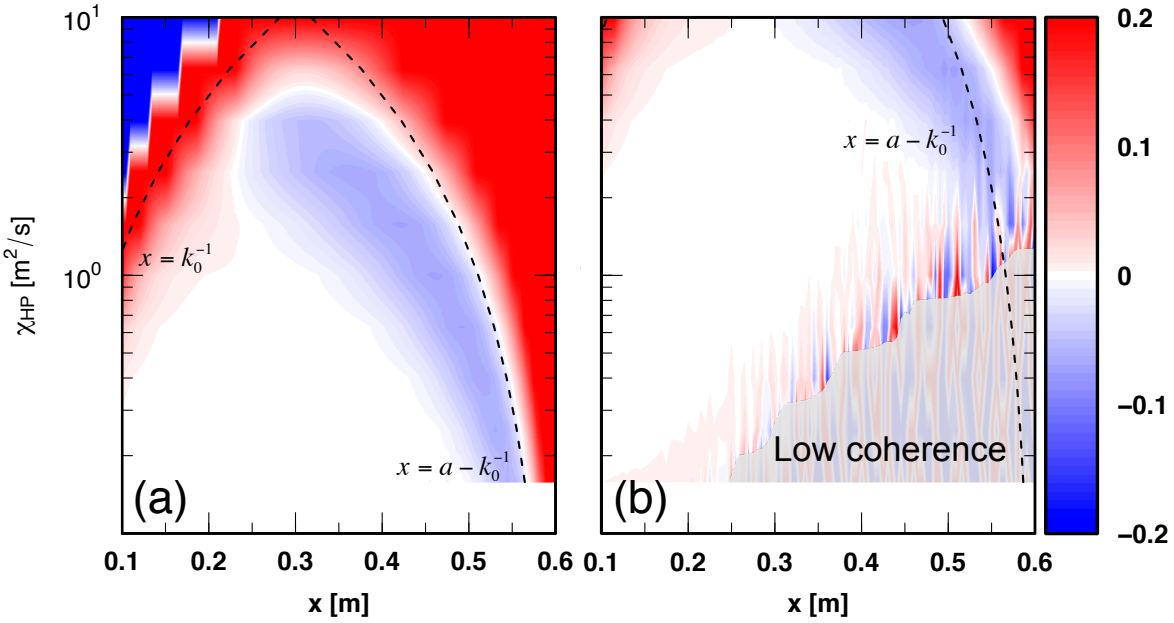

Figure 10. (Color online) Examination for the effect of the edge boundary effect: evaluation error of the imaginary part of the wavenumber at (a) the fundamental MECH frequency and (b) the seventh harmonic frequency.